Cell Reports
Physical Science

CellPress
OPEN ACCESS

Article

Composition-dependent structure and properties of 5- and 15-element high-entropy alloy nanoparticles

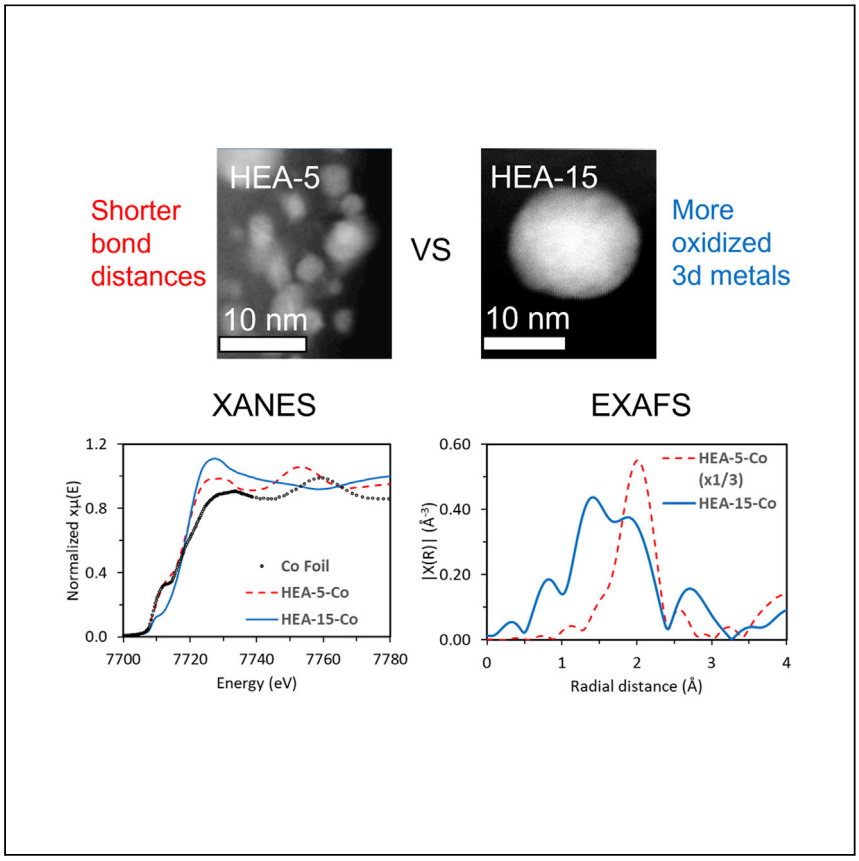

Morris et al. report the variation in the structure and electronic properties of high-entropy alloy nanoparticles when the number of elements is varied between 5 and 15. These findings provide insight into how the structure of high-entropy alloys can be tuned for use in applications such as catalysis.

David Morris, Yonggang Yao, Y. Zou Finfrock, Zhennan Huang, Reza Shahbazian-Yassar, Liangbing Hu, Peng Zhang

binghu@umd.edu (L.H.)
peng.zhang@dal.ca (P.Z.)

Highlights

3d metals show higher oxidation in HEA-15 compared to HEA-5

4d and 5d metals show varied bonding properties between samples

Composition of a HEA plays a key role in the structure and properties observed

Morris et al., Cell Reports Physical Science 2, 100641
November 17, 2021
https://doi.org/10.1016/j.xcrp.2021.100641

Cell Reports
Physical Science

CellPress
OPEN ACCESS

Article

Composition-dependent structure and properties of 5- and 15-element high-entropy alloy nanoparticles

David Morris,[1] Yonggang Yao,[2,3] Y. Zou Finfrock,[4,5] Zhennan Huang,[6] Reza Shahbazian-Yassar,[6] Liangbing Hu,[2,*] and Peng Zhang[1,7,*]

SUMMARY

High-entropy alloy nanoparticles (HEA NPs) are an area of interest due to their interesting structural features, large compositional space, and high potential for catalytic applications. While many HEA NPs have been successfully synthesized and characterized, little is known about the impact of composition on structural features. This work utilizes element-specific X-ray spectroscopy techniques to compare 5- and 15-element HEA NPs with shared elements, aiming to understand the impact that adding additional elements to an HEA has on its structure and properties. Here, we report significant differences between HEA-5 and HEA-15. In particular, the 3d elements show different oxidation behavior associated with different bonding properties. Varied bonding properties are also observed in the 4d and 5d elements. These results provide an understanding of the impact composition plays on the HEA structure, which will serve to aid in the fine-tuning of structure and properties of HEAs through adjusting their composition.

INTRODUCTION

The discovery and characterization of new materials is critical for a wide variety of applications including catalysis and energy storage. Alloys have proven to be an important area in the development of materials, as alloying multiple elements together can offer advantages over more simple single-element systems.[1–3] In particular, high-entropy alloys (HEAs) have emerged as an area of great interest, as they allow for a dramatic increase in the number of elements present within an alloy, giving a much larger compositional space in which potential applications can be discovered.[4–6] HEAs also allow elements with widely varied properties to be alloyed together, overcoming the limitations of more traditional alloy synthesis. One promising synthesis method of HEAs is accomplished through the use of a high temperature pulse, which takes advantage of high entropy to form a well-mixed product despite the widely varied properties of the individual elements.[7] This approach allows for a much large number of elements to be present in the product compared to more traditional synthesis methods, which offers up exciting new possibilities for potential applications. This method allows for HEAs to be successfully formed at the nanoscale,[7] and these HEA nanoparticles (NPs) have been shown to be promising for catalytic applications, making them an exciting area of study.[4,8,9]

In order to gain a proper understanding of HEA NPs, detailed characterization is required. X-ray absorption spectroscopy (XAS) has been widely utilized in the characterization of more traditional alloy NP systems.[10–15] XAS is a powerful technique

[1]Department of Chemistry, Dalhousie University, Halifax, NS B3H 4R2, Canada

[2]Department of Materials Science and Engineering, University of Maryland, College Park, MD 20742, USA

[3]State Key Laboratory of Materials Processing and Die & Mould Technology, School of Materials Science and Engineering, Huazhong University of Science and Technology, Wuhan 430074, China

[4]CLS@APS, Sector 20, Advanced Photon Source, Argonne National Laboratory, 9700 Cass Avenue, Lemont, IL 60439, USA

[5]Science Division, Canadian Light Source, Saskatoon, SK S7N 2V3, Canada

[6]Department of Mechanical and Industrial Engineering, University of Illinois at Chicago, 842 W. Taylor Street, Chicago, IL 60607, USA

[7]Lead contact

*Correspondence: binghu@umd.edu (L.H.), peng.zhang@dal.ca (P.Z.)

https://doi.org/10.1016/j.xcrp.2021.100641

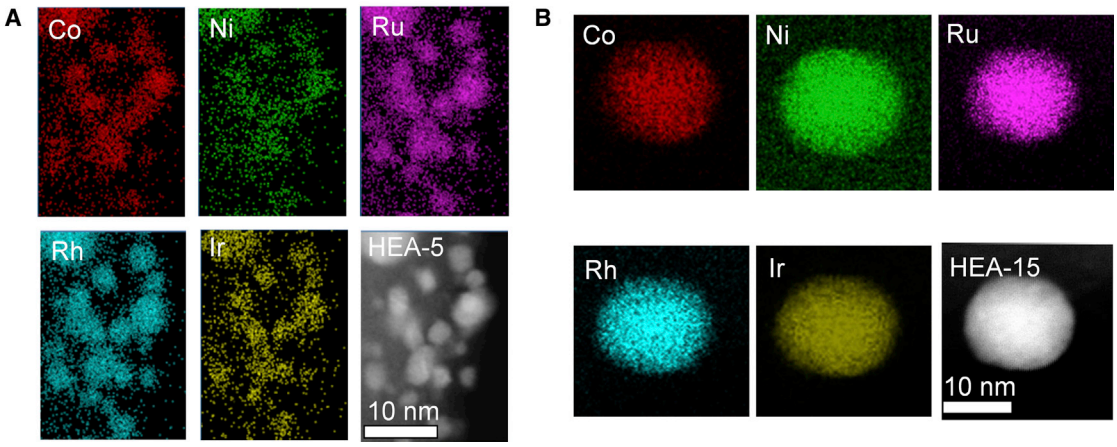

Figure 1. Elemental maps of HEA NPs

(A and B) HEA-5 (A) and HEA-15 (B) elemental maps highlighting the positions of Co, Ni, Ru, Rh, and Ir in the samples. These images show an even distribution of each element across the sample. Scale bar, 10 nm.

that allows for the structure-property relationship of a sample to be determined through a combination of X-ray absorption near-edge structure (XANES) and extended X-ray absorption fine structure (EXAFS). XANES allows for the electronic properties of a sample to be probed, while EXAFS allows for detailed structural information including coordination number (CN) and bond distances to be calculated by fitting a Fourier transformed (FT) EXAFS spectra.[16] Together, these two complimentary techniques allow for a better understanding of a sample to be obtained. XAS is particularly useful for complex HEA systems as it is an element-specific technique, meaning that data can be obtained individually for each element in the sample without heavy interference from other elements.[16] XAS is also an ideal tool for comparing several different samples together, allowing for the impact of a NP's composition to be studied.

Previous studies have utilized XAS to provide characterization of HEA NPs;[8,17] however, little work has been done on directly comparing HEAs and investigating the role that composition plays in the structure and properties they possess. This work focuses on the study of the previously reported Ru-5 MEA-NPs[8] (referred to as HEA-5 in this work) and the 15-HEA nanoalloy[17] (referred to as HEA-15 in this work). These systems share the elements Co, Ni, Ru, Rh, and Ir, which serve as a frame of comparison that will be the main focus of this study. HEA-5 contains an atomic ratio of 20% Co, 20% Ni, 25% Ru, 25% Rh, and 10% Ir.[8] In contrast HEA-15 contains equal amounts of all 15 elements.[17] Both HEA NPs were imaged through scanning transmission electron microscopy (STEM), and elemental maps were generated through energy-dispersive X-ray spectroscopy (EDS) to gain insight into their morphology. XAS measurements were taken for the five common elements, and both qualitative XANES analysis and quantitative EXAFS fitting were conducted, providing structural insight that indicates significant differences between the HEA-5 and HEA-15 NPs.

RESULTS

Imaging of HEA NPs

Characterization was first conducted through STEM and EDS to obtain elemental maps for the HEA NPs, allowing for the distribution of each element in the samples to be clearly observed. The EDS maps for the shared elements in HEA-5 and HEA-15

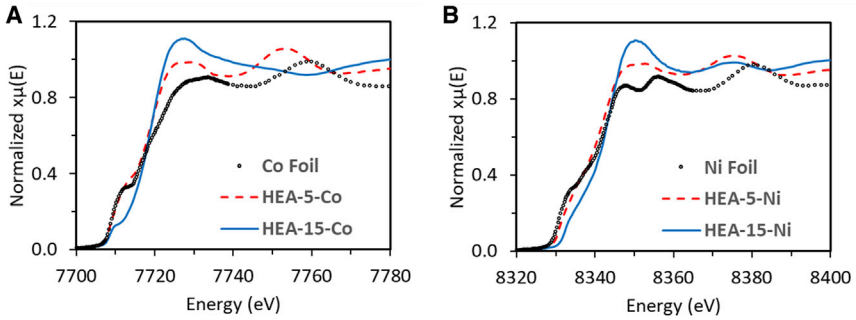

Figure 2. K-edge XANES spectra of 3d elements in HEA NPs

(A and B) Co (A) and Ni (B) XANES spectra of the HEA-5 and HEA-15 samples, along with a metallic foil reference. Variations in the absorption edge intensity and the lack of a pre-edge feature indicate that the 3d elements in HEA-15 are more oxidized than in HEA-5.

are shown in Figures 1A and 1B, respectively. These maps show that each element has a similar distribution across the sample, with a slight preference for the 3d elements toward the outer part of the HEA-15 sample. The only significant difference that can be observed between the two samples is the NP size, which is slightly larger for HEA-15. While these images confirm even distribution of each element across the NP, XAS analysis is required to provide more detailed structural information for these NPs.

Investigation of electronic properties of HEA NPs through XANES

Qualitative comparison of the XANES spectra was conducted to investigate the electronic properties of HEA-5 and HEA-15. The most notable variations in the XANES spectra were observed in the data for Co and Ni, which are the shared 3d elements between the two samples. A comparison of their XANES spectra, alongside a metallic foil reference, is shown in Figure 2. For these elements, the K-edge was measured, which represents an electronic transition from the 1s to the 4p orbital.[18] By analyzing features located prior to and beyond the absorption edge, as well as the absorption edge itself, information regarding the relative oxidation of the element measured can be obtained.[19]

For 3d transition metals, a small "bump," commonly referred to as a pre-edge feature, that is located just before the absorption edge is often observed in samples with metallic character.[20] This feature is located at approximately 7,710 eV for Co and 8,330 eV for Ni. It can be clearly seen in the Co data shown in Figure 2A that HEA-5 possesses this feature, aligning closely with the metallic foil at this point, whereas HEA-15 lacks the feature. In the Ni data, shown in Figure 2B, the difference is not as large, but there is still a deviation between the HEA-5, which is more similar to the foil, and HEA-15. This provides evidence that the HEA-15 is less metallic in character than the HEA-5, which may indicate oxidation of these 3d elements.

This oxidation behavior is further supported by the clear variation in the absorption edge intensity between HEA-5 and HEA-15. A sample with a lower electron density will show a larger absorption edge peak in the XANES spectra.[19] For both Co and Ni, HEA-15 shows a more intense peak at the absorption edge, indicating a lower electron density. This is consistent with the lack of the pre-edge feature, providing further evidence of oxidized Co and Ni in HEA-15. Interestingly, other elements in the samples do not show a significant variation in the XANES spectra (Figures S1

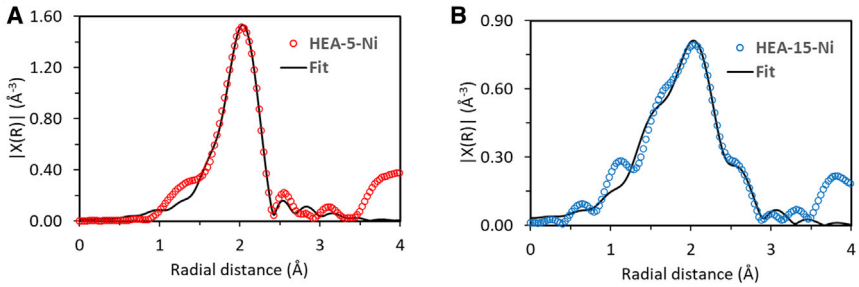

Figure 3. FT-EXAFS spectra and best fit of Ni in HEA NPs

(A and B) HEA-5 (A) and HEA-15 (B) FT-EXAFS spectra for Ni, along with the best fit. HEA-5 shows one dominant peak representing Ni-M interactions, while HEA-15 contains a shoulder peak indicating small amounts of oxidized Ni in the sample.

and S2), which indicates that the apparent oxidation is limited to only the 3d elements in HEA-15.

For all elements, the post-edge features show distinct variation in intensity and position between HEA-5 and HEA-15. These peaks arise from ejected photoelectrons interacting with neighboring atoms in the sample, meaning that they are highly dependent on the atomic structure of the sample.[16,21] This variation is reasonable, as the two samples have a significantly different composition. In order to further investigate the apparent oxidation of the 3d elements in HEA-15, as well as the changes in bonding structure between the samples, quantitative EXAFS analysis was conducted.

Investigation of bonding structure of 3d elements through EXAFS

EXAFS fitting was conducted on the data for Ni, Ru, and Ir in each of the HEA samples, offering representative 3d, 4d, and 5d elements that are shared between the two samples. Figure 3 shows the FT-EXAFS spectra and best fit for the Ni data, and Table 1 shows the bonding parameters determined through EXAFS fitting. Note that the varied intensity in the EXAFS signal between samples is likely caused by a dampening effect of the EXAFS signal caused by varied alloy interactions, rather than significant changes in the CN. Peaks in the FT-EXAFS spectra arise from the interactions of the ejected photoelectron with neighboring atoms in the sample, meaning that different peaks will represent different types of bonds in the sample.[22,23] Therefore, the shape of the FT can provide insight into the bonding environment of each element in the HEA NPs. Due to the similar atomic numbers of Co/Ni and Ru/Rh, as well as the large number of elements in these samples, the fitting of each element used generic M-3d, M-4d, and M-5d fitting paths to account for all the interactions with elements in a specific row of the periodic table.

For Ni, shown in Figure 3, HEA-5 shows a single peak centered around roughly 2.0 Å, which is typical for a Ni-M bond. This spectrum also lacks any significant feature around 1.5 Å, where a peak would be expected to arise from a Ni-O interaction.[24] This is consistent with the XANES, which indicated that the Ni in HEA-5 is metallic in character. In contrast, HEA-15 shows a shoulder peak at approximately 1.5 Å, which is not present in HEA-5, likely indicating a small amount of oxidized Ni. Similarly, in the Co FT-EXAFS spectrum (Figure S3), there is a much more dominant peak representing a Co-O interaction in the HEA-15 data, which indicates that Co is even more susceptible to oxidation than Ni in HEA-15. The EXAFS fitting results for Ni are shown in Table 1. These results confirm the lack of oxidation in HEA-5 and show a relatively small amount of oxidized Ni in HEA-15 with an average Ni-O CN of 2. The CN values also show that neither sample contains a significant number of

Table 1. EXAFS fitting results for Ni

Sample	Bond	CN	R (Å)	σ^2 (Å) x10^{-3}	E_0 (eV)	R factor
Ni foil	Ni-Ni	12 (fixed)	2.481(3)	5.6(4)	−7.7(5)	0.0018
HEA-5	Ni-3d	5.0(6)	2.520(9)	7(2)	−7.6(8)	0.0075
	Ni-4d	2.1(3)	2.54(2)			
HEA-15	Ni-O	2(1)	2.01(4)	9(5)	−9(3)	0.0187
	Ni-3d	5(2)	2.60(2)	12(4)		
	Ni-4d	3(1)	2.63(4)			

Ni-5d interactions. Interestingly, the bond distances for both the Ni-3d and Ni-4d fitting paths are much shorter in the HEA-5 compared to the HEA-15. This may be due to the increased proportion of larger 5d elements in the HEA-15 sample, which would force the 3d elements to form longer length bonds to accommodate these larger atoms in the structure. This trend is consistent with the fitting results of the Ni foil (Figure S5), which show a slightly shorter Ni-Ni bond length than the observed length in HEA-5 for Ni-3d. To provide further insight on this variation observed in the 3d elements, the 4d elements were investigated through EXAFS fitting.

Investigation of bonding structure of 4d elements through EXAFS

Figure 4 shows the FT-EXAFS and best fit for the Ru data, and Figure S6 shows the FT-EXAFS and best fit for Ru foil. Both samples show a set of doublet peaks, with the first around 2.0 Å and the second around 2.5 Å. This kind of doublet in the Ru FT-EXAFS spectra is typical of an alloy interaction between Ru and other metal elements.[25] The second peak in the doublet is far more pronounced in the HEA-15, which indicates a larger CN for the longer distance Ru-M bonds. The EXAFS fitting results for Ru, shown in Table 2, confirm this, as the long-distance Ru-5d fitting path shows a CN of 6 for HEA-15 and only 1.6 for HEA-5. This is likely due to the larger proportion of 5d elements in the HEA-15 sample. The CN values for the Ru-3d and Ru-4d fitting paths show variation between the two samples, as well, unlike the Ni data, which showed consistent CN values. This provides further evidence that the introduction of additional 5d elements beyond Ir, or perhaps the overall higher proportion of 5d elements, significantly changes the local environment of the HEA NPs. Neither sample showed a significant number of Ru-O interactions, which is consistent with the XANES observations (Figures S1 and S2) and indicates that unlike the 3d elements, 4d elements are not oxidized in HEA-15. This is further supported by the FT-EXAFS spectrum of Rh (Figure S4), which shows similar features to the Ru spectra.

As in the Ni data, the bond distances for Ru are much longer in HEA-15 compared to HEA-5. This shows that while the 3d and 4d elements show different behavior in

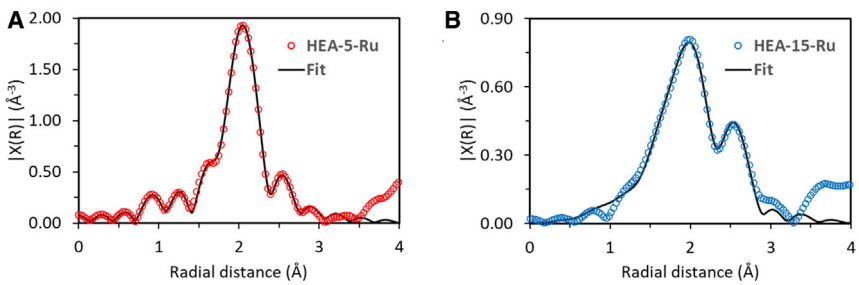

Figure 4. FT-EXAFS spectra and best fit of Ru in HEA NPs

(A and B) HEA-5 (A) and HEA-15 (B) FT-EXAFS spectra for Ru, along with the best fit. The more pronounced doublet peaks in the HEA-15 spectrum indicate a larger amount of longer distance Ru-5d interactions than in HEA-5.

Table 2. EXAFS fitting results for Ru

Sample	Bond	CN	R (Å)	σ^2 (Å) x10^{-3}	E_0 (eV)	R factor
Ru foil	Ru-Ru	12 (fixed)	2.669(3)	2.9(5)	2.9(6)	0.0059
HEA-5	Ru-3d	4.8(7)	2.539(9)	2(2)	0(1)	0.0029
	Ru-4d	2.9(3)	2.55(3)			
	Ru-5d	1.6(3)	2.57(2)			
HEA-15	Ru-3d	2.5(6)	2.61(2)	8(3)	−12(1)	0.0085
	Ru-4d	1.6(6)	2.62(4)			
	Ru-5d	6(2)	2.65(2)			

terms of oxidation, they both share the same trend in bond distances between the two samples. The Ru-3d bond distance was found to be consistent with the Ni-4d bond distance for each sample, providing evidence that the fitting method is accurate and therefore reliable even though each element was fit individually. To obtain further insight, EXAFS fitting was conducted on the Ir data.

Investigation of bonding structure of 5d elements through EXAFS

The FT-EXAFS spectra and best fit for the Ir data are shown in Figure 5, and the FT-EXAFS and best fit for Ir foil is shown in Figure S7. The lack of any significant peak in either spectra around 1.5 Å indicates no significant amount of oxidized Ir in either sample.[26] Like with Ru, a doublet peak structure is clearly seen in the HEA-15 data, which would arise from Ir-M alloy interactions. This doublet is well-pronounced in the HEA-15 with peaks around 2.0 Å and 2.75 Å, but in HEA-5, the second peak is only represented by a very slight shoulder peak. Like in the Ru data, this is likely due to a smaller amount of the longer distance Ir-5d interactions being present in HEA-5. This is confirmed by the EXAFS fitting results, shown in Table 3, as the Ir-5d fitting path has a CN of 1.5 in HEA-5 and 5.0 in HEA-15. Similar to Ru, no significant number of Ir-O interactions were found in the fitting. As in both Ni and Ru, the bond distances for HEA-5 are much shorter than in HEA-15. From these results, it appears that the 5d elements behave similar to the 4d elements in that they don't experience oxidation in HEA-15 but they still experience the increase in bond distance relative to HEA-5. Bond distances for the Ir-4d fitting paths are very consistent with the Ru-5d fitting paths, providing further evidence of accurate and reliable fitting results.

DISCUSSION

As both HEA-5 and HEA-15 were carefully protected from exposure to oxygen (see Experimental procedures) during the XAS measurements, the oxidation observed in the 3d elements for HEA-15 likely occurred due to the composition rather than post-synthesis exposure. One explanation for this observed oxidation

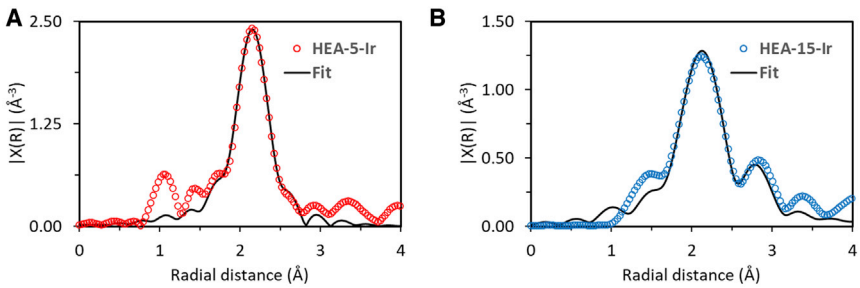

Figure 5. FT-EXAFS spectra and best fit of Ir in HEA NPs

(A and B) HEA-5 (A) and HEA-15 (B) FT-EXAFS spectra for Ir, along with the best fit. The more pronounced doublet peaks in the HEA-15 spectrum indicate a larger amount of longer distance Ir-5d interactions than in HEA-5.

Table 3. EXAFS fitting results for Ir

Sample	Bond	CN	R (Å)	σ^2 (Å) x10^{-3}	E_0 (eV)	R factor
Ir foil	Ir-Ir	12 (fixed)	2.710(7)	2(1)	5(1)	0.0154
HEA-5	Ir-3d	4.4(9)	2.54(1)	2(1)	4(2)	0.0258
	Ir-4d	2.0(5)	2.57(1)			
	Ir-5d	1.5(4)	2.58(2)			
HEA-15	Ir-3d	2.7 (fixed)	2.64(2)	1(1)	5(1)	0.0016
	Ir-4d	1.9 (fixed)	2.65(3)			
	Ir-5d	5.0 (fixed)	2.66(1)			

in the 3d elements is the lattice strain that the 3d elements experience in HEA-15. Compared to the Ni foil, the 3d-3d bond length is significantly longer in HEA-15, which will result in the Ni being destabilized and therefore making it more prone to oxidation. The lattice strain experienced in the 4d and 5d elements is much smaller in comparison, which could explain why they do not experience oxidation in the same manner as the 3d elements.

It has been found that HEA-5 contained several "fragmented domains," which arise from the lattice strain that occurs.[8] As fragmented domains have been linked to high catalytic activity due to the exposure of more active sites, this is an ideal feature for potential catalytic applications.[27] The EXAFS fitting results indicate that in HEA-5 the bond distances are extremely short, which is likely the origin of these fragmented domains. In HEA-15, the bond distances are consistently longer, which is likely due to the increased proportion of 5d elements in the sample. Based on the trend observed in the bond distances, it appears that HEA-15 adapts a lattice structure closer to the bulk for the 4d and 5d elements, whereas HEA-5 adapts a lattice structure closer to the bulk for 3d elements. This difference could explain the higher oxidation states for 3d elements observed in HEA-15.

In summary, this work has provided insight into the impact that the composition of a HEA NP has on its structural features. Through using XAS to analyze the shared elements between HEA-5 and HEA-15, key differences between the structure of the two samples were uncovered. In particular, the 3d elements were found to be greatly impacted by the varied composition, with HEA-15 showing oxidation due to the lowered stability arising from lattice strain. Further study of the 4d and 5d elements supported this mechanism, providing further insight into the composition-dependent bonding properties. All elements showed significantly shorter bond lengths in HEA-5 compared to HEA-15, indicating that the increased proportion of 5d elements forces the adaptation of an alternate structural arrangement. This work demonstrates the impact of composition on the structure of HEA NPs, which will serve to allow for fine tuning the structure and properties of HEA NPs. These findings will ultimately allow for applications in areas such as catalysis.

EXPERIMENTAL PROCEDURES

Resource availability

Lead contact

Further information and requests for resources should be directed to and will be fulfilled by the lead contact, Peng Zhang (peng.zhang@dal.ca).

Materials availability

This study did not generate new unique materials.

Data and code availability

All data reported in this work will be shared by the lead contact upon request.

Synthesis of HEA NPs

HEA synthesis was conducted as reported previously.[7,8,17] The synthesis will be briefly summarized as follows. First, CO_2-activated carbon nanofibers were produced via electrospinning of polyacrylonitrile, which was then stabilized at 260°C for 6 h in air, followed by 1000°C for 2 h in Ar, and finally activated at 750°C for 3 h in CO_2. Each desired metal salt was dissolved in ethanol at a concentration of 0.05 M. Each metal precursor mixture was then deposited uniformly onto the nanofibers at a concentration of approximately 100 μl/cm^2. A rapid high temperature heating pulse at 1,500 K for 500 ms was applied to the substrate by a Keithley 2425 SourceMeter, resulting in the thermal reduction and uniform mixing of the metal salt mixture. After quenching, small, well-mixed NPs were observed to have formed on the substrate.

Imaging

Samples were imaged by SEM (Hitachi SU-70 FEGSEM at 10 kV) and TEM (JEOL 2100F FEG TEM/STEM operated at 200 kV, and JEOL TEM/STEM ARM 200CF). Elemental distribution maps were measured using an Oxford X-max 100TLE windowless X-ray detector. ICP-MS (inductively coupled plasma mass spectrometry) was measured on a PerkinElmer NexION 300D ICP-MS.

XAS measurement and analysis

Ir L_3-edge and Co, Ni, and Ru K-edge XAS data were collected from the CLS@APS (Sector 20-BM) beamline at the Advanced Photon Source (operating at 7.0 GeV) in the Argonne National Laboratory (Chicago, IL, USA). The sample was measured in fluorescence mode simultaneously with a metallic foil reference for each element at room temperature and ambient pressure. Samples were placed in Kapton tape and sealed in an aluminum pouch under Ar gas to protect them from exposure with oxygen. EXAFS data were transformed and normalized into k-space and R-space using the Athena program following conventional procedures.[28] k-ranges of 2.4 to 11.5 Å^{-1} for Ni foil; 2.4 to 12.9 Å^{-1} for HEA-5 Ni; 2.3 to 10.8 Å^{-1} for HEA-15 Ni; 2.6 to 11.7 Å^{-1} for Ru foil; 2.8 to 13.4 Å^{-1} for HEA-5 Ru; 2.1 to 11.0 Å^{-1} for HEA-15 Ru; 2.4 to 9.1 Å^{-1} for Ir foil; 2.6 to 13.6 Å^{-1} for HEA-5 Ir; and 2.3 to 9.9 Å−1 for HEA-15 Ir were used to obtain the FT-EXAFS spectra, with a k weighting of 2. Self-consistent multiple-scattering calculations were performed using the FEFF6 program to obtain the scattering amplitudes and phase-shift functions used to fit various scattering paths within the Artemis program.[28] In the fitting, R-windows of 1.1 to 2.7 Å for Ni foil; 1.5 to 3.4 Å for HEA-5 Ni; 1.0 to 3.0 Å for HEA-15 Ni; 1.0 to 2.8 Å for Ru foil; 1.4 to 3.4 Å for HEA-5 Ru; 1.0 to 3.4 for HEA-15 Ru; 1.0 to 3.3 Å for Ir foil; 1.5 to 3.7 for HEA-5 Ir; and 1.0 to 3.3 Å for HEA-15 Ir were used. In the fitting, E_0 and σ^2 values of each fitting path were correlated together, as indicated by merged cells in the fitting results table, to minimize the number of independent variables and ensure high fitting quality. For the fitting of HEA-15 Ir, the CN values were fixed based on an earlier fitting result to further minimize the number of independent variables due to the short k-range available.

SUPPLEMENTAL INFORMATION

Supplemental information can be found online at https://doi.org/10.1016/j.xcrp.2021.100641.

ACKNOWLEDGMENTS

This research used resources of the Advanced Photon Source, a User Facility operated for the US Department of Energy (DOE) Office of Science by Argonne National Laboratory and was supported by the DOE under contract no. DE-AC02-06CH11357 and the Canadian Light Source and its funding partners. R.S.-Y. acknowledges financial support from National Science Foundation (NSF) award number DMR-1809439.

AUTHOR CONTRIBUTIONS

D.M. and P.Z. contributed to the idea and experimental design. Y.Y. and L.H. synthesized the samples. Z.H. and R.S.-Y. collected high-resolution microscopy results. Y.Z.F. collected XAS measurements. D.M. and P.Z. analyzed the XAS data. D.M. and P.Z. wrote the paper, and all authors commented on the manuscript.

DECLARATION OF INTERESTS

The authors declare no competing interests.

Received: August 12, 2021
Revised: September 24, 2021
Accepted: October 19, 2021
Published: November 4, 2021

REFERENCES

1. Ferrando, R., Jellinek, J., and Johnston, R.L. (2008). Nanoalloys: from theory to applications of alloy clusters and nanoparticles. Chem. Rev. *108*, 845–910.

2. Andrews, M., and O'Brien, S. (1992). Gas-phase "molecular alloys" of bulk immiscible elements: iron-silver (FexAgy). J. Phys. Chem. *96*, 8233–8241.

3. Chen, G., Zhao, Y., Fu, G., Duchesne, P.N., Gu, L., Zheng, Y., Weng, X., Chen, M., Zhang, P., Pao, C.W., et al. (2014). Interfacial effects in iron-nickel hydroxide-platinum nanoparticles enhance catalytic oxidation. Science *344*, 495–499.

4. Batchelor, T., Pedersen, J., Winther, S., Castelli, I., Jacobsen, K., and Rossmeisl, J. (2018). High-Entropy Alloys as a Discovery Platform for Electrocatalysis. Joule *3*, 834–845.

5. Miracle, D., and Senkov, O. (2017). A critical review of high entropy alloys and related concepts. Acta Mater. *122*, 448–511.

6. Ye, Y., Wang, Q., Lu, J., Liu, C., and Yang, Y. (2016). High-entropy alloy: challenges and prospects. Mater. Today *19*, 349–362.

7. Yao, Y., Huang, Z., Xie, P., Lacey, S.D., Jacob, R.J., Xie, H., Chen, F., Nie, A., Pu, T., Rehwoldt, M., et al. (2018). Carbothermal shock synthesis of high-entropy-alloy nanoparticles. Science *359*, 1489–1494.

8. Yao, Y., Liu, Z., Xie, P., Huang, Z., Li, T., Morris, D., Finfrock, Z., Zhou, J., Jiao, M., Gao, J., et al. (2020). Computationally aided, entropy-driven synthesis of highly efficient and durable multi-elemental alloy catalysts. Sci. Adv. *6*, eaaz0510.

9. Xie, P., Yao, Y., Huang, Z., Liu, Z., Zhang, J., Li, T., Wang, G., Shahbazian-Yassar, R., Hu, L., and Wang, C. (2019). Highly efficient decomposition of ammonia using high-entropy alloy catalysts. Nat. Commun. *10*, 4011.

10. Duchesne, P.N., Li, Z.Y., Deming, C.P., Fung, V., Zhao, X., Yuan, J., Regier, T., Aldalbahi, A., Almarhoon, Z., Chen, S., et al. (2018). Golden single-atomic-site platinum electrocatalysts. Nat. Mater. *17*, 1033–1039.

11. Duchesne, P., Chen, G., Zheng, N., and Zhang, P. (2013). Local Structure, Electronic Behavior, and Electrocatalytic Reactivity of CO-Reduced Platinum-Iron Oxide Nanoparticles. J. Phys. Chem. C *117*, 26324–26333.

12. Higaki, T., Liu, C., Morris, D.J., He, G., Luo, T.Y., Sfeir, M.Y., Zhang, P., Rosi, N.L., and Jin, R. (2019). Au_{130-x} Ag_x Nanoclusters with Non-Metallicity: A Drum of Silver-Rich Sites Enclosed in a Marks-Decahedral Cage of Gold-Rich Sites. Angew. Chem. Int. Ed. Engl. *58*, 18798–18802.

13. Zhang, T., Chen, Z., Walsh, A.G., Li, Y., and Zhang, P. (2020). Single-Atom Catalysts Supported by Crystalline Porous Materials: Views from the Inside. Adv. Mater. *32*, e2002910.

14. Walsh, A.G., and Zhang, P. (2021). Thiolate-Protected Bimetallic Nanoclusters: Understanding the Relationship between Electronic and Catalytic Properties. J. Phys. Chem. Lett. *12*, 257–275.

15. Walsh, A., and Zhang, P. (2020). Thiolate-Protected Single-Atom Alloy Nanoclusters: Correlation between Electronic Properties and Catalytic Activities. Adv. Mater. Interfaces *8*, 2001342.

16. Rehr, J., and Albers, R. (2000). Theoretical approaches to x-ray absorption fine structure. Rev. Mod. Phys. *72*, 621–654.

17. Yao, Y., Huang, Z., Hughes, L., Gao, J., Li, T., Morris, D., Zeltmann, S., Savitzky, B., Ophus, C., Finfrock, Z., et al. (2021). Extreme mixing in nanoscale transition metal alloys. Matter *4*, 2340–2353.

18. Chang, J., Lin, B., Hsu, Y., and Ku, H. (2003). Co K-edge XANES and spin-state transition of $RCoO_3$ (R=La, Eu). Phys. B. *329*, 826–828.

19. Bunker, G. (2010). Introduction to XAFS: A Practical Guide to X-Ray Absorption Fine Structure Spectroscopy (Cambridge University Press).

20. Timoshenko, J., and Roldan Cuenya, B. (2021). *In Situ/Operando* Electrocatalyst Characterization by X-ray Absorption Spectroscopy. Chem. Rev. *121*, 882–961.

21. Frenkel, A.I. (2012). Applications of extended X-ray absorption fine-structure spectroscopy to studies of bimetallic nanoparticle catalysts. Chem. Soc. Rev. *41*, 8163–8178.

22. Simms, G.A., Padmos, J.D., and Zhang, P. (2009). Structural and electronic properties of protein/thiolate-protected gold nanocluster with "staple" motif: A XAS, L-DOS, and XPS study. J. Chem. Phys. *131*, 214703.

23. Ankudinov, A., Ravel, B., Rehr, J., and Conradson, S. (1998). Real-space multiple-scattering calculation and interpretation of x-ray-absorption near-edge structure. Phys. Rev. B Condens. Matter Mater. Phys. *58*, 7565–7576.

24. Wang, H., Miller, J., Shakouri, M., Xi, C., Wu, T., Zhao, H., and Akatay, M. (2013). XANES and EXAFS studies on metal nanoparticle growth and bimetallic interaction of Ni-based catalysts for CO_2 reforming of CH_4. Catal. Today *207*, 3–12.

25. Omajali, J.B., Gomez-Bolivar, J., Mikheenko, I.P., Sharma, S., Kayode, B., Al-Duri, B., Banerjee, D., Walker, M., Merroun, M.L., and Macaskie, L.E. (2019). Novel catalytically active Pd/Ru bimetallic nanoparticles synthesized by *Bacillus benzeovorans*. Sci. Rep. *9*, 4715.

26. Nong, H., Reier, T., Oh, H., Gliech, M., Paciok, P., Vu, T., Teschner, D., Heggen, M., Petkov, V., Schlögl, R., et al. (2018). A unique oxygen ligand environment facilitates water oxidation in hole-doped $IrNiO_x$ core-shell electrocatalysts. Nat. Catal. *1*, 841–851.

27. Wang, L., Zeng, Z., Gao, W., Maxson, T., Raciti, D., Giroux, M., Pan, X., Wang, C., and Greeley, J. (2019). Tunable intrinsic strain in two-dimensional transition metal electrocatalysts. Science *363*, 870–874.

28. Ravel, B., and Newville, M. (2005). ATHENA, ARTEMIS, HEPHAESTUS: data analysis for X-ray absorption spectroscopy using IFEFFIT. J. Synchrotron Radiat. *12*, 537–541.